SCISPACE
formerly Typeset

Open access • Journal Article • DOI:10.1021/ACS.JPCA.7B12297

The Production of Methane, Acetone, "Cold" CO and Oxygenated Species from IsoPropyl Alcohol in a Non-Thermal Plasma: An In-Situ FTIR Study — Source link

Paul A. Christensen, Zeinab T. A. W. Mashhadani, Abd Halim Bin Md Ali, Michael A. Carroll ...+1 more authors

Institutions: Newcastle University, University of Manchester

Published on: 17 Apr 2018 - Journal of Physical Chemistry A (American Chemical Society)

Topics: Nonthermal plasma, Isopropyl alcohol, Isophorone and Catalysis

Related papers:

- Use of a non-thermal plasma for the production of synthesis gas from biogas
- Mechanistic aspects of plasma-enhanced catalytic methane decomposition by time-resolved operando diffuse reflectance infrared Fourier transform spectroscopy
- A kinetic study of the oxidation of acetonitrile: A model for NO formation from fuel-bound nitrogen
- The active oxygen for direct oxidation of methane to methanol in the presence of hydrogen
- A Molecular Beam Mass-Spectrometric Study of Isopropyl Nitrate Pyrolysis Reactions at Short Residence Times and Temperatures up to 700 K

Share this paper:

View more about this paper here: https://typeset.io/papers/the-production-of-methane-acetone-cold-co-and-oxygenated-4kkhk4meij

Newcastle University

ePrints

Christensen P, Mashhadani Z, MdAli AHB, Carroll M, Martin P.
The Production of Methane, Acetone, "Cold" CO and Oxygenated Species from Isopropyl Alcohol in a Non-Thermal Plasma: An In-Situ FTIR Study.
***The Journal of Physical Chemistry* 2018, 122(17), 4273–4284.**

Copyright:

This document is the Accepted Manuscript version of a Published Work that appeared in final form in The Journal of Physical Chemistry, copyright © American Chemical Society after peer review and technical editing by the publisher. To access the final edited and published work see https://doi.org/10.1021/acs.jpca.7b12297

Date deposited:

03/05/2018

Embargo release date:

17 April 2019

Newcastle University ePrints - eprint.ncl.ac.uk

This document is confidential and is proprietary to the American Chemical Society and its authors. Do not copy or disclose without written permission. If you have received this item in error, notify the sender and delete all copies.

The Production of Methane, Acetone, "Cold" CO and Oxygenated Species from Isopropyl Alcohol in a Non-Thermal Plasma: An In-Situ FTIR Study

Journal:	*The Journal of Physical Chemistry*
Manuscript ID	jp-2017-12297z.R2
Manuscript Type:	Article
Date Submitted by the Author:	n/a
Complete List of Authors:	Christensen, Paul; Newcastle Univ, School of Engineering Mashhadani, Zeinab; Newcastle Univ, School of Engineering Md Ali, Abd Halim Bin; Newcastle University, School of Engineering Carroll, Michael; Newcastle Univ, School of Natural and Environmental Sciences Martin, Philip; University of Manchester, School of Chemical Engineering & Analytical Science

SCHOLARONE™
Manuscripts

The Production of Methane, Acetone, "Cold" CO and Oxygenated Species from IsoPropyl Alcohol in a Non-Thermal Plasma: An In-Situ FTIR Study

Paul A. Christensen[*a], *Z. T. A. W. Mashhadani*[a], *Abd Halim Bin Md Ali*[a], *Michael A. Carroll*[b] *and Philip A. Martin*[c]

[a]School of Engineering, Bedson Building, Newcastle University, Newcastle upon Tyne, UK, NE1 7RU

[b]School of Natural and Environmental Sciences, Bedson Building, Newcastle University, Newcastle upon Tyne, UK, NE1 7RU

[c]School of Chemical Engineering and Analytical Science, The University of Manchester, Oxford Road, Manchester, M13 9PL

Abstract: This paper reports *in-situ* Fourier Transform InfraRed (FTIR) spectroscopic studies on the non-thermal plasma reaction of isopropyl alcohol in dinitrogen at Macor (a ceramic containing oxides of Al, Mg and Si) and the analogous thermally-driven process. Whilst isopropyl alcohol did not react at the Macor at temperatures up to 600°C, the study of the non-thermal plasma-driven process at the ceramic led to unexpected chemistry hitherto not observed, primarily the reaction of IPA in dinitrogen at short timescales to produce methane, HCN, acetone and "cold" CO at ca. 115K. The CO, methane and HCN rapidly established steady state concentrations, pointing to the need for faster FTIR studies: at longer times, isophorone and a "polymethylacetylene-like" polymer were formed as a brown oil. The observation of the steady-state gases and brown oil suggested parallel pathways in the plasma, the latter taking place at the plasma/catalyst interface, and the former in the plasma remote from the catalyst. Replacing dinitrogen with argon completely inhibited or negated the production of the oil, had no effect upon the processes taking place in the plasma remote from the Macor and instead resulted in the production of acetylene.

1. Introduction

Non-thermal plasma

Plasma is widely regarded as the fourth state of matter and is characterized by the presence of atoms, molecules, ions, electrons and radicals having internal energies (with the exception of the electrons) unevenly distributed over the three degrees of freedom.[1] The dielectric barrier discharge reactors typically utilising Non Thermal Plasmas (NTPs) generally consist of two electrodes across which is a pulsed or AC high voltage field separated by one or more dielectric

layers. In such plasmas, the temperature of the electrons is as high as 10^3 – 10^4 K, whilst the heavier species remain around ambient temperature.[2]

The role of the dielectric and catalyst in a non-thermal plasma

Initially, the gap between the two high voltage electrodes in NTP reactors was packed with dielectric pellets such as Al_2O_3 or $BaTiO_3$ and these were employed simply to increase the non-uniformity of the electric field so that there are regions of much higher electric field than the applied field thus leading to more energetic electrons. The discharge current I as described by the Manley equation:[3]

$$I = 4 f C_d (V - V_o C_g/C) \quad (1)$$

where f is the discharge frequency, C_d is the dielectric capacitance, C_g is the capacitance of the background gas within the discharge gap, V_o is the discharge onset voltage and V is the discharge voltage (kV). It was then found that certain dielectrics could also act as catalysts, steering the reaction to yield different products with different catalysts (e.g. Ni/SiO_2 [4], NiO/WO_3 vs Faujasite vs Mordenite[5,6]) but the trends observed when using a range of such catalysts are simply not understood.[4,7,8] Consequently, this led to catalyst selection for NTP processes being based on identifying those materials that are active for the same chemical processes when carried out in conventional, thermal reactors operating under steady state conditions; however plasmas are most certainly not in a steady state and such materials are generally found not to be especially catalytic in NTP systems.

The potential advantages of plasma catalytic chemistry

The ions, radicals and vibrationally electronically excited species produced through the collisions between the high energy electrons generated in the NTP are only observed at temperatures > 1000 K in thermal systems.[9] In addition, the vibrationally excited species present in NTPs, and essentially unavailable in thermal systems, can exhibit enhanced sticking probabilities at catalyst surfaces and hence enhance the reactivity of endothermic processes.[9,10] Thus the key advantage of non-thermal plasma chemistry is that it makes a range of chemistries viable, where, by conventional means, they would require extremes of temperature and/or pressure that would be technically challenging and economically unfeasible. In addition, in principle, almost 97% of the plasma discharge power of low temperature plasmas can be converted into vibrational excitation of the gas feed molecules.[11] In summary, coupling NTP with catalysts offering novel chemical pathways with lower activation energies opens up the potential for a wholly new and exciting field of chemistry. In addition, it should be possible to enhance targeted reactions and suppress others by appropriate choice of catalyst, and feed gas, by controlling the number density of electrons and controlling the temperatures of the electrons and gaseous species.

A significant challenge of NTP-driven systems is perceived to be the high energy demand; however, companies such as Siemens (private communication) have adopted strategies involving the harnessing of the spillover of renewably-generated electricity to the production of fuels and chemical products as matching the production of electricity from renewable energy to demand is very difficult, and often the surplus is simply spilled. The storage of this surplus energy chemically is seen as a possible solution to this problem; for example, the plasma-driven

reduction of CO_2 to CO and O_2 is perceived as one possible chemical process, particularly as some industrial plants produce almost pure CO_2 as waste gas.[12] There could also be environmental benefits associated with plasma technology: thus, Martuzevicius and co-workers[13] compared conventional technologies with plasma systems for the destruction of volatile organic compounds, and found that NTP-based technology performed better with respect to the ozone layer depletion, acidification, eutrophication and human toxicity potential. The authors reported that "The relatively high demand of electrical energy causes lower positioning of plasma technologies in cases where no other materials are utilized and major waste is formed. On the other hand, many traditional end-of pipe technologies are associated with high amounts of process waste, which provides plasma technologies with an opportunity to establish them in the market as more efficient and in many occasions, more environment-friendly ones".

Finally, as discussed below, plasma catalysis has not been researched sufficiently to exploit its very real potential.

A summary of the applications of non thermal plasma

There are many companies producing commercial non-thermal plasma systems across a range of applications and these include: Enercon, Alternor, Plasma Etch, AcXys (surface treatment/etching) and Ozonia, Lenntech and Evoqua (ozone for water treatment). Further, electrostatic precipitation for industrial separation and gas cleaning dates back to 1907 [14]; however, none of these commercial systems rely upon plasma catalysis.

In the laboratory, topical chemical conversions using NTPs include[15]: ozone generation[16], the conversion of CH_4 to H_2 and C2-C4 derivatives[17], toluene to phenol and cresols[5], CO_2 and H_2O to syngas and synfuels[18], the treatment of Volatile Organic Compounds[19], decontamination and disinfection[20], the deep desulfurization of diesel fuels[21], the treatment of flue gas[22] and the dry reforming of CO_2 and CH_4.[23]

Typically, the reactors employed in the above systems are based on cylinders of Al_2O_3 or quartz with one high voltage electrode wrapped around the outer surface of the cylinder and a metal rod, mounted along the axis of the cylinder, as the second electrode.[24-26] Where catalyst pellets are used packed bed reactors are generally employed.[25]

The challenges facing the exploitation of plasma catalytic chemistry

As stated above, the potential of NTP-assisted catalysis in chemical synthesis is as yet largely unrealized: this is most likely due to the lack of analytical information on the processes taking place at the catalyst/plasma interface (interestingly, the US Plasma 2010 Committee report[27] concluded that the interactions of plasmas with solid surfaces is one of the six critical challenges that define the plasma research frontier; a view that is still extant today). Hence the chemical mechanisms and kinetics involved are simply not understood.[28,29] This is reflected in the paucity of catalyst selection as discussed above and the simplicity (and unoptimised nature) of NTP reactor design.[9,11]

As stated above, NTP reactors utilising catalyst are most commonly of the packed-bed type, either as a variant of the tube reactors described above with the gap filled with the

catalyst/dielectric pellets or two plate electrodes separated by a gap filled with pellets.[10] It is not at all clear these configurations are optimum, as there is no theoretical basis for their design: such a basis requires the chemistry taking place in the reactor to be modelled. All designs so far have essentially been empirical; they have not as yet been formulated on the basis of known or estimated rate constants or reaction mechanisms. The interaction of highly excited and reactive species with solid surfaces is largely unknown both in terms of the chemistry and the timescale over which such reactions take place.[9] Furthermore, whilst the potential synergy between NTP and catalysis is widely acknowledged in the NTP community, it has not been possible to include catalysis in models: indeed, even accounting for chemical reactions on the chemically simple surfaces of the HV electrodes has proven too challenging[30] due to the lack of chemical information on the species present. For example, in the absence of information on the identities of the species present in non-thermal plasmas, and at the solid (dielectric/catalyst)/plasma interface, all possible species need to be included in the model (e.g. up to 150 molecules[31,32]) which increases computing time and decreases the accuracy of the model. Our previous FTIR research strongly suggests that it should be possible to provide the hard experimental data required to aid effective modelling and hence reactor design.[33]

The plasma-driven conversion of isopropyl alcohol at Macor

The overall aim of the NTP work in Newcastle is to study plasma catalytic processes by employing *in-situ* infrared spectroscopy to probe the plasma glow region (the region of the plasma that emits the characteristic blue/white glow) and the plasma/catalyst interface, and hence determine the mechanisms of such processes. This information will then be compared to data obtained using a Specac Environmental Chamber and Diffuse Reflectance InfraRed

Spectroscopy attachment[34] allowing the catalyst to be monitored *in-situ* using diffuse reflectance IR spectroscopy at temperatures up to 600 °C. The same reactants and catalysts will be studied in both systems. Hence Macor was chosen as the catalyst for our initial studies as it has both a reasonable dielectric constant (ca. 6) and high thermal stability.[35] The Macor was not characterized as it is produced only in pellet form which is extremely hard and hence it has not proved possible to produce contaminant-free powder for, for example, XRD or XPS by filing etc.

The initial system chosen for comparative study was IsoPropyl Alcohol (IPA) for two reasons: (1) its relevance to the study of the removal of Volatile Organic Compounds (VOCs) from air. IPA is a routinely-employed solvent in the electronics industry and, as such, a number of studies have been reported in the literature on the removal of this Volatile Organic Compound (VOC) from air using NTP-assisted catalysis.[36-38] (2) We already have IR data on the thermal behaviour of SnO_2 [34], and there is a wealth of IR data in the literature on the interaction of IPA with oxide surfaces under thermal conditions, see for example.[39-46] The carrier gas employed in the studies reported in this paper was nitrogen rather than air in order to start with the simplest system comprising only two components.

The state-of-the-art in in-situ FTIR studies of non-thermal plasmas

Whilst the plasma/catalyst surface has not been investigated extensively with *in-situ* infrared spectroscopy, such studies have started to appear, There are a number of studies on the downstream analysis of the exhaust from NTPs, see for example[47], but actual studies of the plasma glow with IR spectroscopy[33] or of the catalyst surface in contact with a plasma is only a recent phenomenon.[48-53] The quality of the information that can be obtained from in situ FTIR is

exemplified by the work of Li and co-workers on the deposition of Si from hexamethyldisiloxane plasma[49], Rivallan and colleagues on the conversion of IPA at Al_2O_3 [48], Stere et al. [50] on the hydrocarbon assisted NOx removal from simulated diesel fuel over silver-based catalysts, Rodriguez et al. [51] on the conversion of IPA at Al_2O_3, CeO_2 and TiO_2 and Jia and Rousseau on the plasma-assisted reaction of acetone at CeO_2 [52]. These studies employed the Diffuse Reflectance approach[50,51], transmission through the catalyst as a wafer[48,52] or passed the IR beam through the plasma glow above the solid surface[47,49]. Rivallan and co-workers[53] employed the step scan approach to study the gas phase reduction of CO_2 in a tube reactor (i.e. they did not study the catalyst/plasma interface): however, they saw no reaction products or intermediates, although the authors did achieve a time resolution of ca. 400 μs.

In general, and even in the presence of ozone[54], the plasma-driven catalysed conversion of IPA generally leads to toxic products such as acetone and mesityl oxide rather than complete conversion to CO_2, and hence the requirement for effective catalysts is clear.

Justification for the work

The preliminary work reported in this paper seeks to determine, compare and contrast the mechanisms of the plasma catalytic and thermal catalytic conversions of IPA at Macor as a first step in understanding the chemistries taking place at the plasma/catalyst surface with the ultimate aim of devising appropriate, optimum catalysts to realize the potential of NTP-assisted catalysis.

2. Experimental

Isophorone (3,5,5-trimethyl-2-cyclohexen-1-one, 97%) and isopropyl alcohol (99.5%) were supplied by Sigma Aldrich and used without further purification. Nitrogen gas was supplied via cryogenic boil-off.

IR spectra of liquid isopropyl alcohol and isophorone were obtained using a Presslok holder (Thermo Scientific); ca. 50 μL of the liquid was placed between two 25 mm dia. 2 mm thick CaF_2 windows (Crystran) in the holder.

The non-thermal plasma infrared cell

The non-thermal plasma infrared cell, see Figure S1, was designed and fabricated in-house and was made from a 15 cm long, cylindrical polyteTraFluoroEthylene (PTFE) tube with an outer diameter of 6.3 cm and an inner diameter of 2.5 cm. The high voltage electrodes were in the form of two plungers, sealing against the inner walls of the PTFE via rubber 'O' rings. One plunger was hollow down its axis (a 5 mm diameter hole) and the feed gas was delivered via this channel and removed via an outlet nozzle in the top of the cell. The electrodes were covered with 5 mm thick Macor caps fitted snugly over each disc electrode, with a hole aligned with the central, gas delivery channel. Two infrared transparent CaF_2 windows (25 mm diameter, 3 mm thick, Crystran) were glued into the PTFE cell. The distance between the windows (path length) was 5.1 cm. The windows were positioned such that their centres aligned with the centre of the 5 mm gap between the electrodes. The plasma volume was 7.4 cm^3 and the residence time at a flow rate of 200 cm^3 min^{-1} was 2.2 s.

The electrodes were connected to a NeonPro lamp transformer, NP100000-30 (Hyrite, China) which provided an output up to 10 kV at a constant frequency of 24 kHz. A voltage controller (Carroll & Meynell) was used to control the input power to the HV transformers. The input power to the plasma was monitored using a Gadget 13A (N67FU Maplin, UK) Power Meter; the input powers quoted were those obtained by subtracting the input power observed with plasma from the reading obtained with the system switched on but with no plasma initiated (4 W).

The FTIR plasma system

An Agilent FTS7000 FTIR spectrometer with a Deuterated Tri-Glycine Sulfate (DTGS) detector was employed. The IR beam was passed through the plasma via the two CaF_2 windows to the detector via an Amtir-1 filter, 25mm × 2mm (Spectra-Tech, USA) to remove visible light.

The IsoPropyl Alcohol (IPA) was supplied by Sigma-Aldrich (99.5%) and used without further purification. Isopropyl alcohol vapour was delivered to the chamber of the reflectance accessory by bubbling nitrogen gas through the alcohol held in a Dreschel bottle. The cell was first flushed with N_2 at a flowrate of 200 cm^3 min^{-1} for 120 minutes; when the system was stable, a background spectrum was collected. N_2 was then bubbled through the IPA and admitted to the cell at a total flow rate of 200 cm^3 min^{-1}. A reference spectrum (S_R, 100 co-added and averaged scans at 4 cm^{-1} resolution, 100 seconds per scan set) was collected in the absence of plasma. Sample spectra, S_S, were then taken as a function of time after the high voltage power supply was switched on, and at regular intervals thereafter up to 20 minutes. The spectra are presented as:

$$\text{Absorbance, } A = \log_{10} (S_R/S_S) \qquad (2)$$

These results in difference spectra in which peaks pointing upwards (i.e. to + absorbance) represent a gain in absorbing species at S_S with respect to S_R, and peaks pointing down (to – absorbance) represent the loss of absorbing species. In order to remove unchanging absorptions, spectra were subtracted with subtraction factors employed as necessary.

The concentrations of the various species observed were calculated using the Beer-Lambert law:

$$A = \varepsilon c L \qquad (3)$$

where: ε is the molar decadic extinction coefficient (M^{-1} cm^{-1}), c = concentration (M) and L = optical path length (5.1 cm). This data manipulation results in difference spectra in which peaks with positive amplitude arise from the gain of absorbing species in S_S with respect to S_R, and peaks with negative amplitude to the loss of absorbing species.

The temperature of the Macor caps of the transmission cell were monitored at an input power of 27W using a RS-1327 IR Thermometer C infrared thermometer gun in experiments conducted without FTIR data collection (as the cover to the sample compartment had to be removed), the temperature of the Macor caps were found to increase to ca. 43°C over 20 minutes. This measurement was not possible with the plasma reflectance cell for safety reasons as the cell could not be manipulated and the thermometer gun would not fit into the sample compartment.

However, the reflectance cell did employ a cooling gas stream. We have also simulated the absorption band shapes of some of the heavy species in the plasma[55] and it suggests that the rotational temperatures are usually between ambient and up to around 100°C depending on the chemical system, the deposited power and the plasma duration.

We have not observed any problems from the proximity of the high voltage power supply to the FTIR spectrometer: the shielding employed thus appears to work well. Occasionally, we observe "spikes" on the spectra obtained using the reflectance cell, an observation still under investigation, and this was remedied by repeating the experiment.

The spectra presented below were highly reproducible and stable. Essentially the same data were obtained over a number experiments spread over 8 months. For example, as is described in the paper (see figure S7), the experiments were repeated as a function of power, and the same features and species observed, except in varying relative amounts. Again, as is discussed in the paper, the species observed after 1 minute were confirmed (with the exception of HCN and addition of acetylene) in the Argon experiment which was carried out some 11 months after the initial IPA experiments using nitrogen.

We did not observe any carbon deposits in the plasma experiments on the windows or walls of the cells, or on the Macor; however, this is not to say it does not occur as it may be swept out of the plasma cell by the feed gas.

The FTIR thermal system

In-situ FTIR thermal experiments were carried out using a Varian 670-IR spectrometer equipped with a ceramic air-cooled infrared source, a DLaTGS detector and a Specac environmental chamber and diffuse reflectance unit (see[34] for details) with the IR beam reflected from a 12.5 mm diameter, 2 mm thick Macor disc. The Specac reflectance accessory allows IR spectra to be collected under controlled atmosphere conditions from room temperature to 600 °C and pressures from vacuum to 34 atm. The IR beam was incident on the sample in the cell at angles from 20° to 76° with respect to the horizontal plane via a ZnSe window. The same data manipulation was employed as described above in equations (1) and (2).

Water was removed from both the spectrometer purges by a NITROSource generator and to the FTIR cells from a cylinder (N5.5 100%, BOC). The absence of water from atmosphere of the spectrometer and the cells was confirmed by examining the single beam spectra as well as by following the spectra of the cells as a function of time to check that they were free from water vapour prior to commencing the experiments. Water may have been released from the surface of the Macor during the experiments described below, but there was no direct evidence from the FTIR measurements (distinctive fine structure centred around 3750 and 1640 cm^{-1}) to support this release.

Extinction coefficients

The extinction coefficient of CH_4 was determined from measurements using the pure gas in a 1 cm pathlength cell and is presented in Table 1 along with that of the 3335 cm^{-1} band of HCN which was estimated from the paper by Choi and Barker.[56]

Table 1. The extinction coefficients of various gas phase species. See text for details.

	Peak /cm^{-1}	ε /M^{-1} cm^{-1}
CH_4	3086	3.5
	1346	6.2
HCN	3335	2.8

We estimate that the detection limit for CO was ca. ≥ 1.0 x 10^{-5} M in the thermal cell and a factor of five lower in the plasma transmission cell.

3. Results and Discussion

The thermal experiments

Figure 1 shows spectra collected during an experiment in which a Macor disc was heated from 25 to 600 °C in an atmosphere of IPA vapour and nitrogen gas. The reference spectrum (S_R) was collected at 25 °C and the temperature then ramped at 5 °C min^{-1}, sample spectra (S_S) collected at 50 °C and further spectra collected every 50 °C up to 600 °C. For clarity, only the spectra collected every 100 °C are shown.

As can be seen from Figure 1, there are loss features at 3340, 2976, 2887, 1481, 1232, 1007 and 950 cm^{-1} that increase steadily in intensity as the temperature was increased. In addition, there are loss and gain features between ca. 3600 and 3770 cm^{-1}. The bands between 3600 and 3770 cm^{-1} and loss features at 3340 cm^{-1}, 1481 and 1232 cm^{-1} also appear in a repeat of the experiment in Figure 1 in the absence of IPA: hence these bands may be attributed to the surface chemistry of the Macor. The 3340 cm^{-1} feature may reflect the dehydration of surface OH

groups and the bands between 3600 and 3770 cm^{-1} changes in the nature and coverage of isolated O-H moieties[34]. The features at 2976, 2887, 1007 and 950 cm^{-1} are due to the loss of adsorbed IPA.[39,41,44,45,48,51,57] Of significance is the fact that there are no obvious product features.

The plasma experiments

The plasma experiments were carried out at 18, 20, 22, 24, 26 and 27 W (the plasma became unstable at 28 W). The various product features observed were the same in all the experiments.

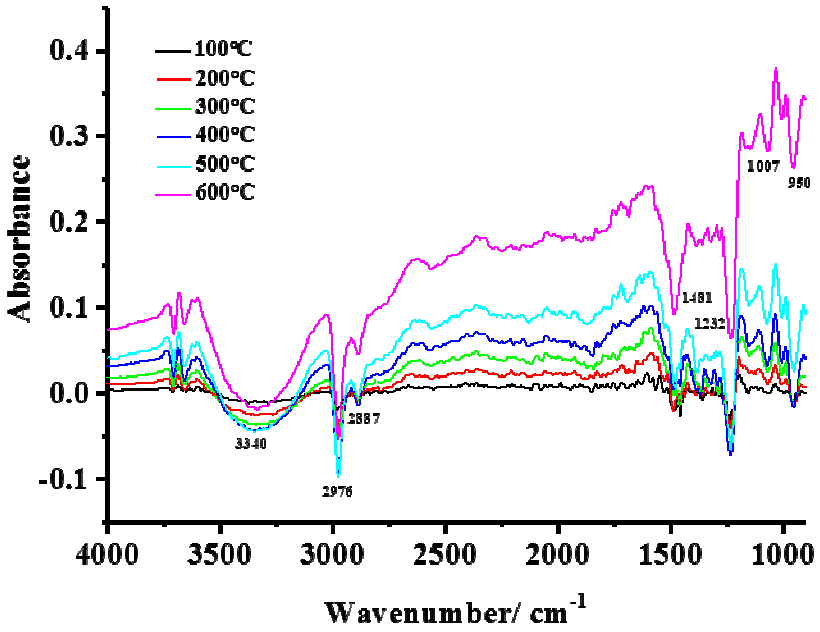

Figure 1. FTIR spectra (100 co-added scans and averaged scans at 4 cm^{-1} resolution, ca. 120 seconds per scan set) collected from a 12.5 mm diameter, 2 mm thick Macor disc in a static atmosphere of isopropyl alcohol vapour in nitrogen gas during an experiment in which the reference spectrum was taken at 25 °C; the temperature was then ramped up at 5 °C min^{-1} and sample spectra collected every 50 °C from 50 °C to 600 °C.

The spectra collected at 1 minute

Spectral acquisition commenced 1 minute after initiating the plasma: this period was chosen simply to allow some time for the system to settle, rather than assuming the plasma had reached steady state. Figure 2(a) shows the spectra collected after 1 minute during a series of experiments carried out as a function of input power (see the discussion around Figure S6 below), the reference spectra in each case being collected of the IPA-containing N_2 gas without plasma. As expected, the figure is dominated by loss features due to gas phase IPA; see Figure S2, which compares spectra of liquid and gas phase IPA, and Table 2 which lists the various features. As can be seen from Figure S2, the 3657, the doublet at 1472 and 1462 and the distinctively-shaped band at 1251 cm^{-1} are characteristic of the gas phase IPA, whilst the cluster of bands at 1160, 1130 and 1111 cm^{-1} and single, sharp feature at 952 cm^{-1} are characteristic of the liquid phase IPA. It is clear from Figure 2(a) that there is vibrational structure on the high frequency side of the IPA C-H loss features on all the spectra, as well as gain features below ca. 2250 cm^{-1}; however, these are obscured by the strong loss features due to gas phase IPA. Hence, in order to highlight any small features, the gas phase IPA spectrum was subtracted from the spectrum collected at 27 W in Figure 2(a), using the 3657 cm^{-1} O-H feature in the gas phase spectrum to determine the scaling factor to ensure annulling of the IPA bands; the result is shown in Figure 2(b) and the various features so observed summarized in Table 3.

The gain features at 3335 cm^{-1} and 3284 cm^{-1} may be attributed to the P and R branches of HCN:[56] these features were present on all the spectra collected after 1 minute operation. The fine structure centred on 3086 cm^{-1} and the sharp band at 3016 cm^{-1} in Figure 2(a) may be unambiguously attributed to the P and Q branches of the ν_3 band of CH_4, and the sharp feature at

Table 2. The IR absorptions of gas and liquid phase isopropyl alcohol.[39-42,45,48,51,57]

Gas phase IPA /cm^{-1}	Liquid phase IPA /cm^{-1}	Assignment
3657	3347	ν_{OH}
2980		ν_{aCH3}
2971	2971	ν_{aCH3}
2933	2932	ν_{sCH3}
2900 (sh)		
2886	2883	ν_{CH}
1472	1466	δ_{aCH3}
1462		δ_{aCH3}
	1408	
1383	1379	δ_{sCH3}
	1340	
	1310	
1251		δ_{OH}, δ_{CH},
1152	1160	ν_{CC}, ν_{CO}, r_{CH3}
	1130	
	1111	
1080(sh)		ν_{CC}, r_{CH3}
1073		ν_{CC}, r_{CH3}
966		Terminal and bridged C-O str.
954	952	
942(sh)		

Table 3. The features in Figure 2(b). See text for details.

/cm^{-1}	Assignment
3335 + 3284	HCN
2732 + 2705	?
2164 + 2130	"Cold" CO
1666	Isophorone
1740	Acetone
1369	Acetone
1215	Acetone
3086 + 3016	P and Q bands of ν_3 band of CH_4
1305	Q branch of ν_4 band of CH_4

1305 cm^{-1} to the ν_4 band of CH_4 [58] by comparison with an authentic sample of CH_4 in 13.4% CH_4+ 10.6% CO_2 + 76.0% N_2, see Figure S3, the Q branch in Figure 2(b) is distorted by the IPA C-H loss feature.

The bands at 1740 cm^{-1}, 1369 and 1215 cm^{-1} may be attributed to gas phase acetone[59] an assignment confirmed by comparison with the IR spectrum of an authentic sample. Thus, Figures S4(a) and (b) show the spectrum in Figure 2(b) and a spectrum of gas phase acetone obtained by placing ca. 0.1 cm^3 of the liquid in the plasma transmission cell and allowing it to evaporate. As well as the C=O band at 1740 cm^{-1} and the band at 1369 cm^{-1} the features at 1130, 1217 and 1228 cm^{-1} form a highly distinctive group which may be unambiguously assigned to acetone. It is clear from Figures S4(a) and (b) that the broad feature around 3347 cm^{-1}, the features at 2968 and 2978 cm^{-1}, the multiple bands around 1130 cm^{-1} and the feature at 1046 cm^{-1}

are not due to acetone. With the exception of the 1046 cm^{-1} feature which remains unassigned, these bands may be attributed to liquid IPA condensing on the cell windows, and this is discussed in detail below as is the origin of the broad feature at ca. 1666 cm^{-1}.

There are at least two possible routes to acetone: the dehydrogenation of IPA over metal and metal oxide catalysts is a well-known endothermic[60] and important reaction requiring temperatures ≥ 200 °C catalysed by basic oxides including MgO [60-63]; hence it may be that the acetone is produced in an analogous process involving the removal of dihydrogen from the H of the hydroxyl group and an H atom on the carbon adjacent to the CHOH moiety. However, such a surface process would be inhibited by the formation of the liquid film, and the data below suggest that the formation of acetone is linked to that of CO and HCN, hence it is more likely that the acetone is produced from an entirely gas-phase process; for example, from mass spectrometry studies of IPA, acetone can be produced by deprotonation of $C_3H_7O^+$.[64]

It does not seem unreasonable to assign the bands at 2164 and 2130 cm^{-1} to the P and R branches of a linear molecule. In addition, the reasonably high frequency of the band centre suggests a light molecule; further the band centre is identical to that of gas phase CO (2145 cm^{-1}), see Figure S5 which shows the features in Figure 2(b) compared to an authentic sample of CO. The 2164 and 2130 cm^{-1} bands resemble the P and R branches of CO, except with a reduced bandwidth, as would be expected if the molecule was cooled down: for example, Bauerecker et al. [65] observed the rotation-vibration bandwidth of $^{13}C^{16}O$ to be reduced by about 40% on cooling the gas from 300 K to 45 K, without any change in band centre. From Figure S5, the bandwidth is ca. 24% lower than that of CO at room temperature, and a calculation based

on separation of the maxima of the P and R branches[66] suggest a temperature of ca. 115 K, in broad agreement with the work of Bauerecker and co-workers; if the resolution is taken into account, this gives a temperature range of 89 – 143K. This is a challenging observation as it would be expected that the gas phase molecules in the plasma glow would be in thermal equilibrium: however, it may simply be the case that the cold CO bands represent the steady state of the species, constantly produced and constantly removed by the gas feed.

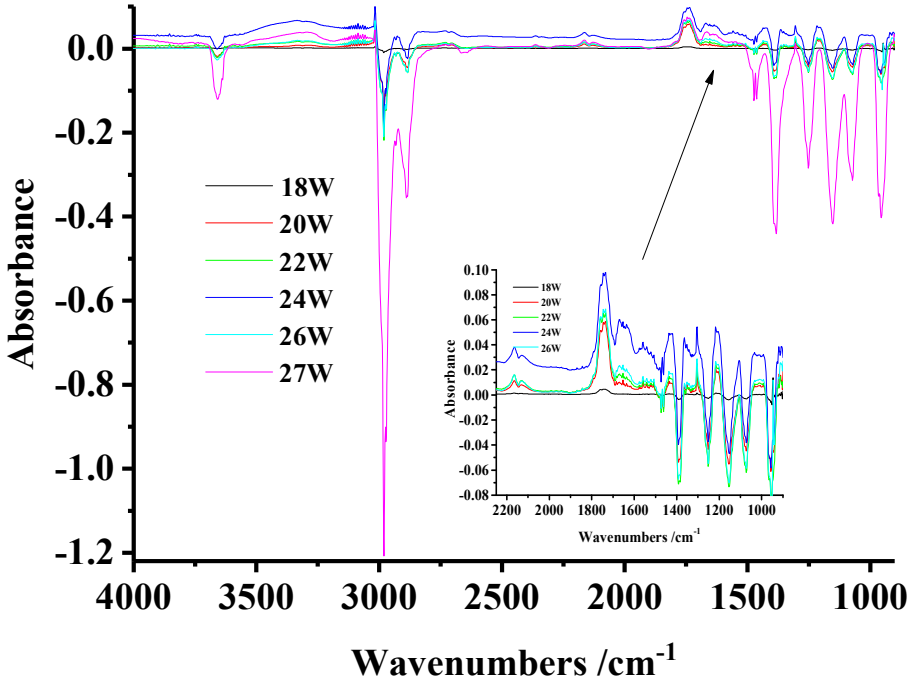

(a)

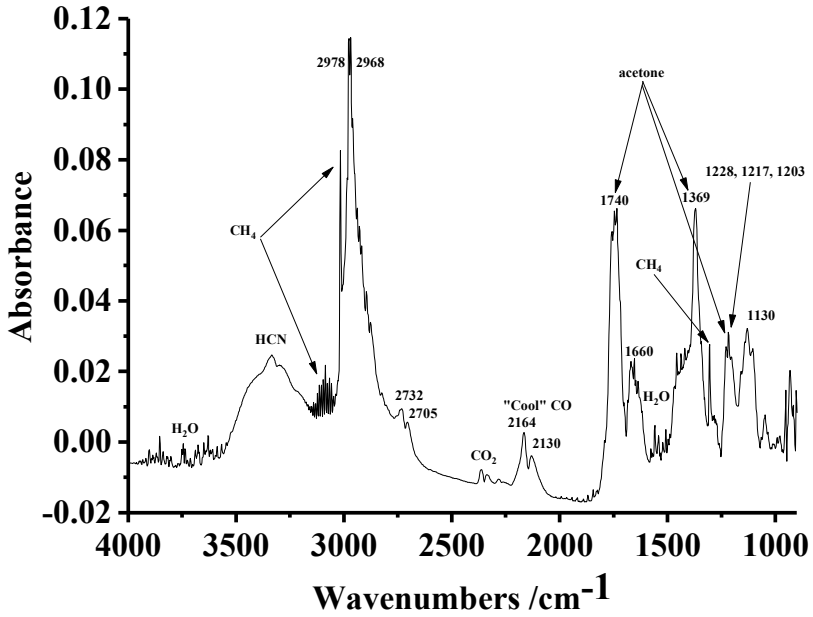

(b)

Figure 2. (a) FTIR spectra (100 co-added scans and averaged scans at 4 cm^{-1} resolution, ca. 100 seconds per scan set) collected during experiments in which nitrogen gas was passed through isopropyl alcohol at 298K and atmospheric pressure into the IR plasma transmission cell at a flow rate of 200 cm^3 min^{-1} and a reference spectrum collected. The plasma was then initiated sample spectra collected as a function of time. The spectra shown were collected after 1 minute at the various input powers shown. The inset shows the spectra below 2200 cm^{-1} without the spectrum taken at 27W, for clarity. (b) The spectrum collected at an input power of 27W in Figure 2(a).

Figure S6 shows typical spectra collected at an input power of 27 W using the spectrum collected without plasma as reference: as can be seen, the CH_4 and CO bands (boxed) are present, and their intensities unchanged throughout the experiment indicating steady-state

concentrations: this postulate was supported by the IPA/Ar data discussed below. The HCN features also do not change in intensity with time and hence were annulled when the spectrum collected at 1 minute was subtracted from those collected at longer times, (see Figure 4) and discussion below. It did not prove possible to determine the behaviour of the acetone due to the overlying strong features.

Figure 3 shows plots of the partial pressure of methane, and the absorbances of the CO band at 2164 cm^{-1} and the 1740 cm^{-1} acetone band normalised to their maximum values, as a function of input power, measured from the spectra collected after 1 minute and using the spectra collected without plasma as the background. The raw data are presented in Figure S7. As can be seen, all three species apparently track each other, suggesting they are formed via a common intermediate and/or in the same process, and this postulate was supported by the experiment discussed below in which N_2 was replaced by Ar.

In the plasma transmission cell, the IR beam passed along the surfaces of both the Macor caps, but bands attributable to adsorbed IPA were not observed in any of the spectra recorded using the cell.

The spectra collected at longer times

Figure 4 shows the spectrum collected after 1 minute in Figures 2(a) and S6 subtracted from those taken at longer times in order to remove the loss features due to gas phase IPA; as may be

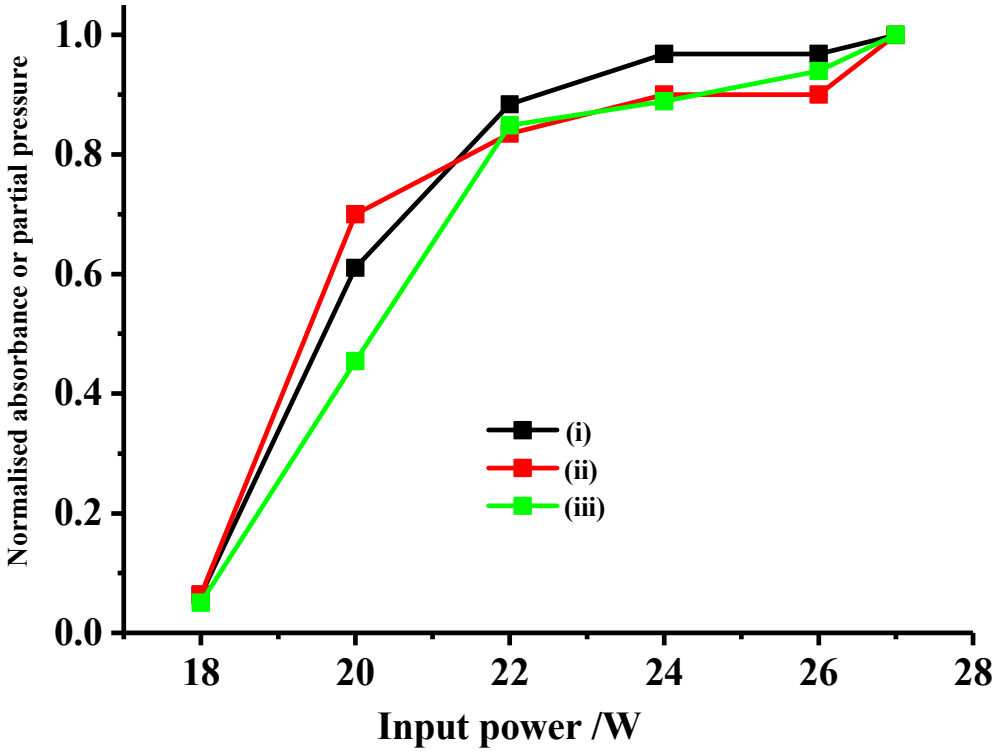

Figure 3. Plots of (i) the absorbance of the 2164 cm^{-1} CO band, (ii) the partial pressure of CH_4 and (iii) the absorbance of the 1740 cm^{-1} acetone band, measured after 1 minute plasma operation as a function of input power from the experiments shown in Figure 2(a). The plots were normalised to their maximum values.

seen from the figure, there is no further reduction in the vapour pressure of the IPA as a function of time once the power to the plasma is switched on. Following the experiment depicted in the figure, a brown oily deposit was observed on the Macor plates and CaF_2 windows, which was also observed in all the plasma experiments using IPA and nitrogen, and the IR spectrum of which corresponded closely to the spectrum collected after 20 minutes in Figure 4. As will be discussed further below, this oil appeared to comprise at least two components, A and B. The oil

was dissolved in $CdCl_3$ and an attempt was made to analyse it with carbon and proton NMR, but the results were inconclusive

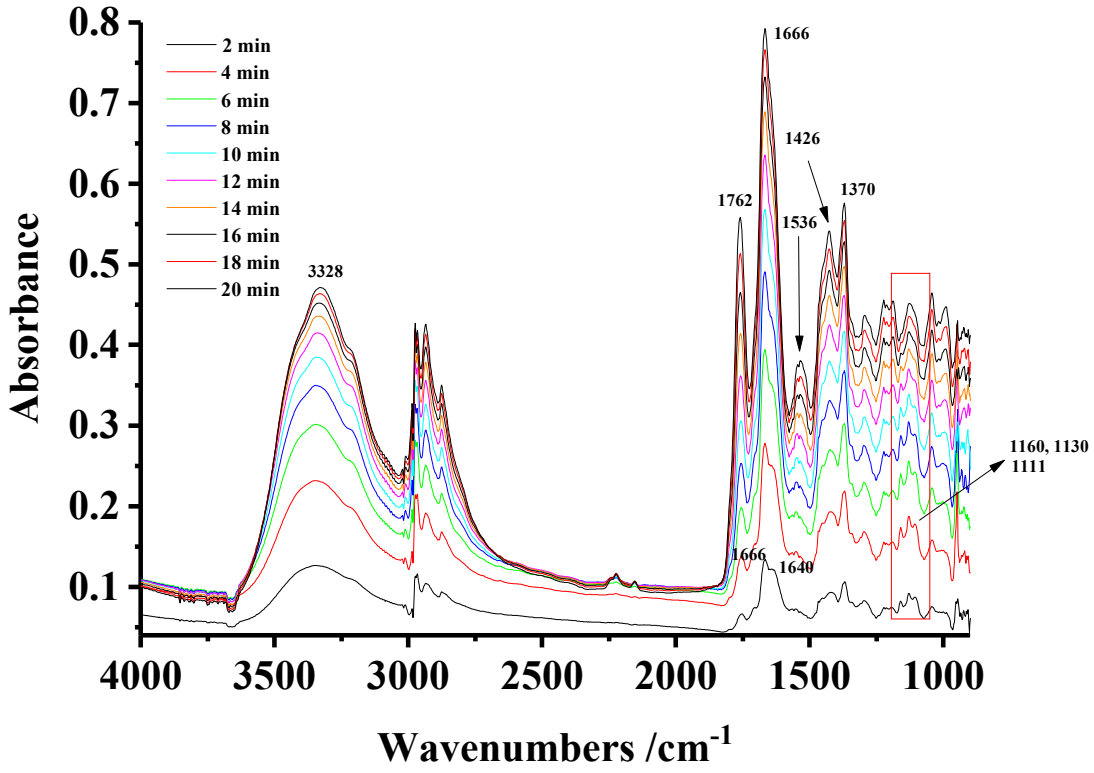

Figure 4. The spectra obtained during the experiment carried out at 27W shown in Figure 2(a). The spectra were collected using a gas feed of IPA vapour in N_2. The N_2 was bubbled through pure IPA at 298K at a flow rate of 200 cm^3 min^{-1}. The reference spectrum was collected under the same conditions, but without plasma. The spectrum collected after 1 minute was subtracted from those taken up to 20 minutes.

Figure 5 shows plots of the key features in Figure 4 as a function of time normalized to their maximum values, and Figure S8 shows the raw data. As can be seen from Figures 4 and 5, the 1762 and 1536 cm^{-1} bands track each other and may thus be assigned to a single species; it is

also clear that the 1666, 1426 and 1370 cm^{-1} features do not belong to the same species as the 1762 and 1536 cm^{-1} bands. Unfortunately, the 1426 and 1370 cm^{-1} bands are in the spectral region where significant overlap of bands from different species may be expected. This challenge is addressed further below.

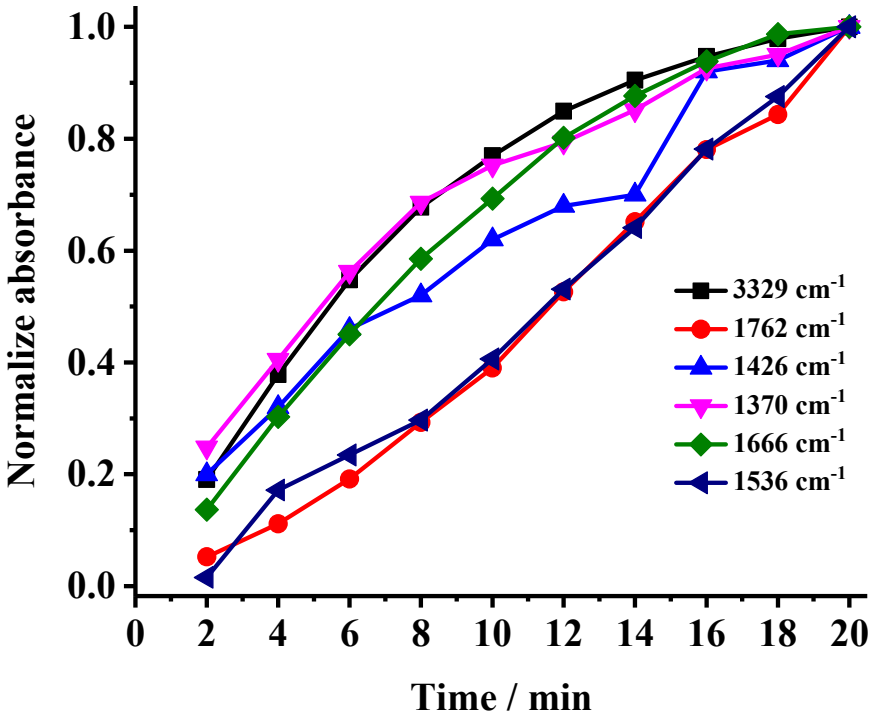

Figure 5. Plots of the intensities of the key features in Figure 4 as a function of time, normalized to their maximum values.

Close inspection of Figure 4 shows the distinctive 1160, 1130 and 1111 cm^{-1} bands attributable to liquid phase IPA, suggesting condensation on the windows and surfaces of the cell, which become indistinct in the spectra collected after 8 minutes. These bands do not appear to change in intensity significantly up to 8 minutes, suggesting the thickness of the condensed layer does not change over this timescale. These observations suggest that the spectra in Figure 4 could be

simplified if divided into two regions, those up to 8 min from which was subtracted the spectrum collected after 1 minute, and the spectrum taken at 8 minutes subtracted from those taken up to 20 minutes. The results are shown in Figures S9 and S10.

By comparing the relative intensities of the various features in Figures S9 and S10 it is clear that there are bands due to at least two different species, some isolated as discussed above, but some clearly overlapping in the spectral region below 1500 cm^{-1}. Figure 6 shows the spectra collected at 8 minutes in Figure S9 and that at 20 minutes in Figure S10 along with the spectrum of liquid IPA in Figure S2 scaled such that the 1130 cm^{-1} feature is approximately the same intensity as that in Figure S9. It is clear that the peak at 2970 cm^{-1} in Figures 6 and S9 is due to liquid IPA, that there is a significant contribution from liquid IPA to the broad feature between 2500 and 3700 cm^{-1} in the spectra collected up to 8 minutes and that there are features below 1500 cm^{-1} belonging to both the unidentified species characterized by the strong bands at 1762 and 1666 cm^{-1}. The situation becomes clearer if the spectra collected at 10 min and 20 min in Figure S10 are compared, see Figure 7; thus the 1762, 1536, 1426 and 1370 belong to one species, species A, and the 1666, 1630(sh), 1430, 1385 and 1373 cm^{-1} features to species B. It is not clear from the various figures what species is responsible for the 3329 cm^{-1} absorption: thus from Figure 6 it can be seen that there is an appreciable contribution from the O-H stretch of liquid IPA to the O-H absorption up to 8 minutes, and there are marked differences in the shape of the feature between the two NTP spectra in the figure. Further, it appears from Figure 6 that the 2936 and 2876 cm^{-1} C-H bands are common to both species A and B, if in different relative intensities. The various features are summarised in Table 4. The time-dependent behaviour of

the intensities of the 1426 and 1370 cm^{-1} species A bands in Figure 5 is clearly distorted by the presence of the underlying 1430, 1385 and 1373 cm^{-1} features of species B.

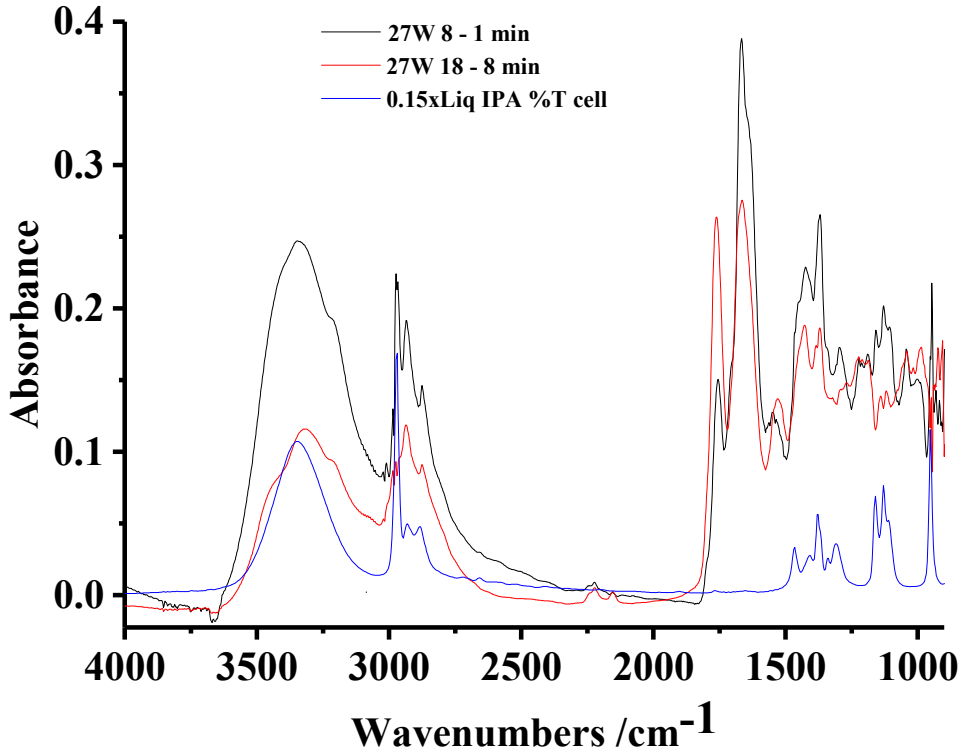

Figure 6. A comparison of the spectrum (i) collected after 8 minutes in Figure S9, (ii) the spectrum taken after 20 minutes in Figures S10, and (iii) the spectrum of liquid IPA in Figure S2. See text for details.

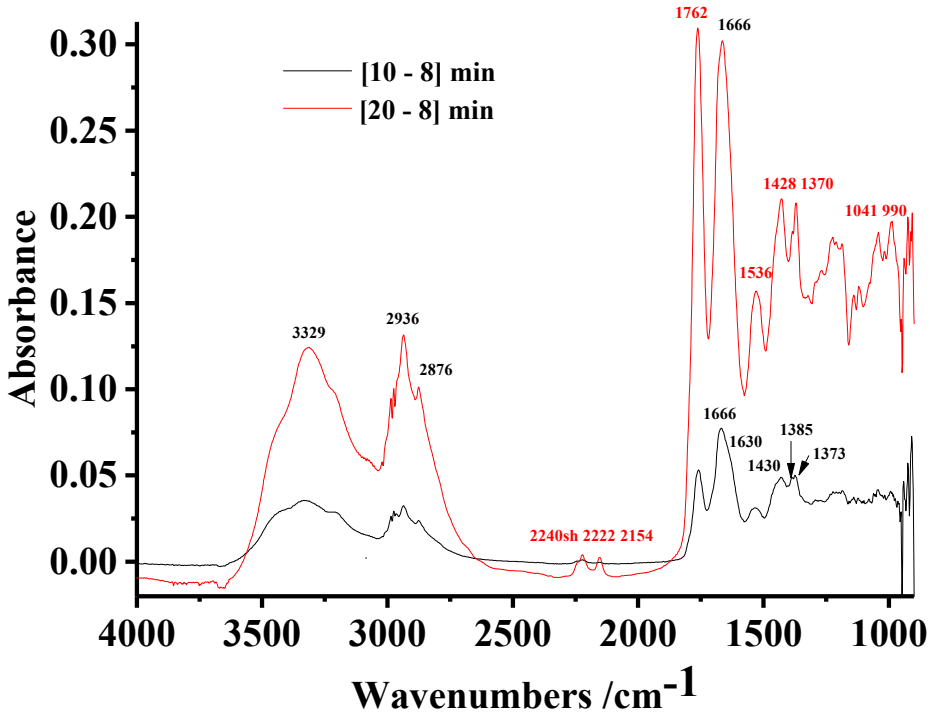

Figure 7. The spectra collected after (i) 10 minutes and (i) 20 minutes in Figure S10. See text for details.

The acetone generated from the IPA may undergo a range of transformations leading to higher molecular species bearing both C=O and –OH groups such as β-hydroxyketones (acid and/or base catalysed Aldol reaction) and diols resulting from Mg catalysed Pinacol coupling. The nature and distribution of the products is dependent upon the catalyst employed as is the extent of similar downstream reactions with additional structural complexity due to facile dehydration of these materials installing random elements of unsaturation. This sequence of events inevitably produces an orange or red polymeric oil[67,68] containing CH_3, C=O, C=C and O-H groups. The number, distribution and nature of these functionalities are a result of both the catalyst and the experimental conditions employed, and the polymers produced are described generically as

"polymethylacetylene-like". The C-H asymmetric and symmetric stretches are observed at ca. 2960 and 2865 cm^{-1}, respectively, and the absorptions due to C=O conjugated with the polyene structure appear around 1705 and 1670 cm^{-1}, the latter much stronger than the former. The C=C stretch of the polyene backbone moves down in frequency as the conjugation increases, see[69] and references therein, and was reported to absorb around 1560 cm^{-1} in the seminal work by Cataldo.[67,68] If the conjugation between the ketone C=O moieties and the polyene backbone is broken, often by cyclisation and/or the formation of quaternary carbon centres (e.g. geminal CMe_2 groups), the polyene C=C absorption does not shift, but the C=O absorption moves to significantly higher frequencies. The fact that N_2 (along with Macor and IPA) is essential to the formation of the liquid film suggests that nitrogen-containing moieties are also present in the polymer. Thus we suggest that species A is a polymeric product resulting from a cascade of Aldol/Pinacol/dehydration type reactions initiated by the formation of acetone. Trinh and Mok[70] investigated the oxidative decomposition of acetone over ZnO and/or MnO_2 catalysts and observed the formation of a brown polymeric deposit on the walls of their reactor. The IR spectrum of this deposit shows similarities to the spectra in Figure 4, and the authors postulated the polymer contained ester groups.

In the thermally-driven Aldol condensation of acetone over alkaline catalysts, as well as polymethylacetylene-like products, isophorone is a common side product (e.g. from cyclisation and subsequent E_{1CB} elimination of water). Figure S11 shows the spectrum of an authentic sample of isophorone, and the absorptions are summarized in Table 4. On the basis of the spectrum, we identify product B as isophorone. Interestingly, isophorone is one of the products

Table 4. The features observed in the spectra in Figures 4 and S6, S9 & S10, and the absorptions of isophorone from Figure S11.

Product A bands /cm^{-1}	Product B bands /cm^{-1}	Isophorone /cm^{-1}
2936	2936	2957
2876	2876	2869
1762	1666	1668
1536	1630 (sh)	1630
1426	1430	1435
1370	1385	1378
	1373	1367

from the thermal Aldol condensation of acetone at lamellar double hydroxides which, as is the case with Macor, also contain magnesium and aluminium oxides.[71]

Close inspection of the spectrum collected after 2 minutes in Figure 4 shows that the OH band is prominent, as is a clear band at 1640 cm^{-1}. The latter does not track the adjacent 1666 cm^{-1} and becomes overlain by the 1630 cm^{-1} shoulder. The presence of the 1640 cm^{-1} and the broad O-H absorption, along with the sloping absorption that increases at frequencies > 1750 cm^{-1} and the clear, broad absorption underlying the bands below 1750 cm^{-1} suggest the formation of water[72], along with C-OH groups: the former arising from the Aldol condensation reaction.

The production of the gas phase products CO, CH_4 and HCN, and the fact that they fairly rapidly attain a steady-state in the plasma in the flowing feed gas, in conjunction with the

separate production of the isophorone and the polymer–containing brown oil, which requires a longer time to form, suggests the presence of two separate and parallel reaction pathways. This observation is in accord with the model of Kim et al. [73] in which the active species such as OH radicals occupy a thin layer perhaps 50 μm thick above the catalyst and are available for reaction at the catalyst: above this layer, species produced in the plasma react in the same way as in the absence of catalyst. Thus the gas phase products are produced in the body of the plasma, away from the direct participation of the catalyst, whilst the isophorone and polymer are produced in the plasma adjacent to the catalyst: both possibly require the build-up of intermediates on the Macor, but, as may be seen from the plots in Figure 5, the isophorone is produced in a different process to the polymer, and more rapidly.

Replacing nitrogen with argon

Figure 8(a) shows the spectra obtained in an analogous experiment to that in Figure 4 except that the nitrogen feed was replaced by argon. The plasma was initiated at a significantly lower power (8 W in contrast to 18 W using N_2) and the spectra in Figure 8(a) were collected at 8 W. The most obvious difference between the two experiments, apart from the expected absence of HCN in Figure 8(a), was that no liquid film or isophorone was produced, clearly highlighting the importance of nitrogen gas in their formation. Cold CO, at 136 K (allowing for the resolution gives a temperature range of 108 – 167 K) was also produced. Figure 8(b) shows the spectrum collected after 1 minute in Figure 8(a) with the IPA bands annulled by subtraction, using the O-H stretch at 3657 cm^{-1} to determine the scaling factor. The acetone bands are clear, as are the CO_2, cold CO and methane absorptions.

In addition to the bands stated above, there are features at 3315 and 3263 cm^{-1} in Figures 8(a) and (b) which may be attributed to the C-H stretch of acetylene.[74] Along with the inhibition of the film formation, the production of acetylene strongly suggests the existence of a modified mechanism on employing argon.

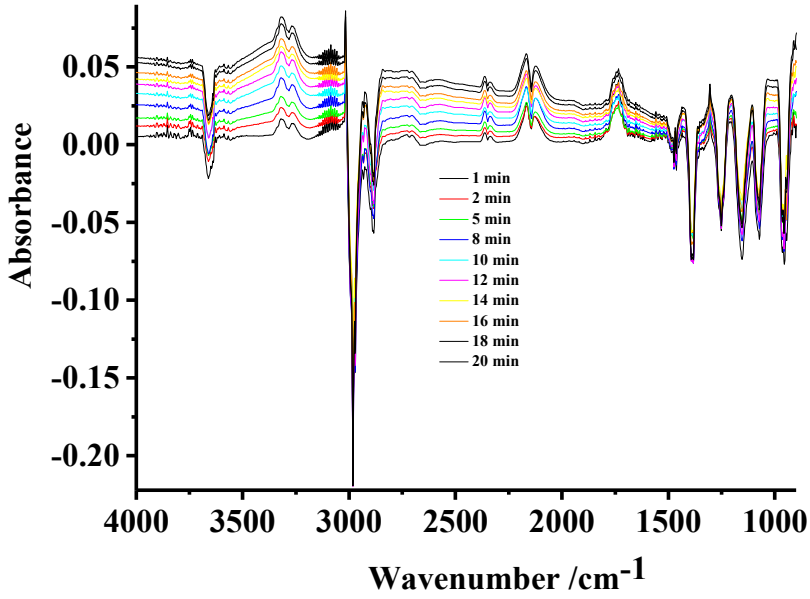

(a)

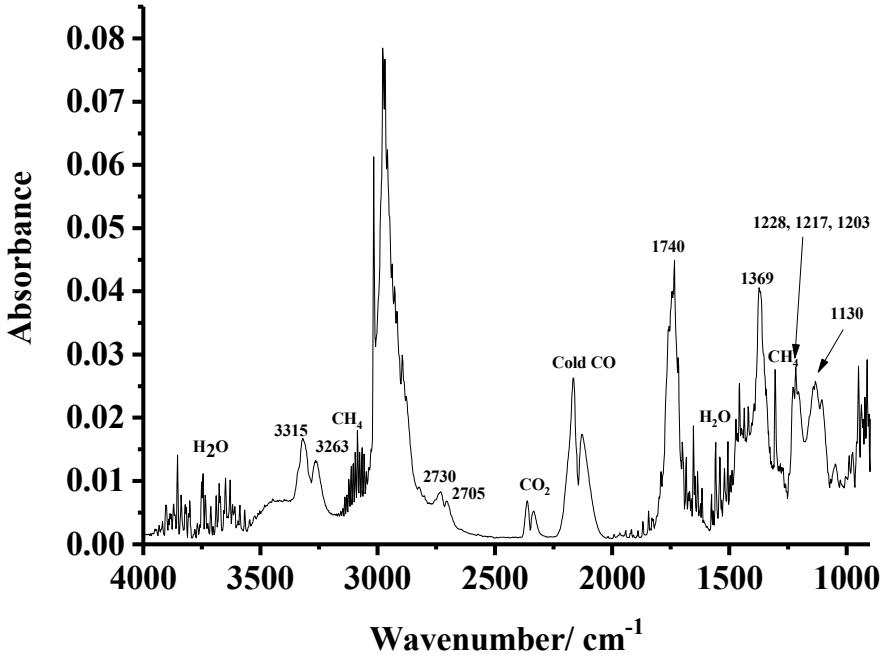

(b)

Figure 8. (a) The spectra collected in an analogous experiment to that in Figure 4, except that the feed gas was argon and the input power 8W. (b) The spectrum collected after 1 minute in Figure 8(a). The gas phase IPA bands were annulled using the spectrum of pure IPA, and employing the O-H stretch of the IPA at 3657 cm^{-1} to determine the subtraction factor.

Figure 9 shows plots of the various features in Figure 8(a) as a function of time. As was stated above, it is clear that (1) the methane, cold CO, CO_2 and acetone essentially show steady state concentrations (as was noted above), whereas the acetylene in the plasma glow steadily increases, and (2) with the exception of the acetylene the remaining species clearly track each other, suggesting they arise from the same or linked process(es). From the figure, the steady state partial pressure of methane was ca. 12 mBar, i.e. not insignificant. The oscillating nature of the plots in Figure 9 are fascinating, but their interpretation requires further study.

The proposed mechanism

First it will be useful to review the key facts arising from the data discussed above:

- It is clear that cold CO, CH_4, HCN and acetone are produced in the plasma glow in the first minute.

- From Figure S6 and numerous repeats, it is clear that CH_4 and cold CO (at least) are produced for the full 20 minutes i.e. the formation of the liquid has no effect therefore their formation must take place entirely in the gas phase.

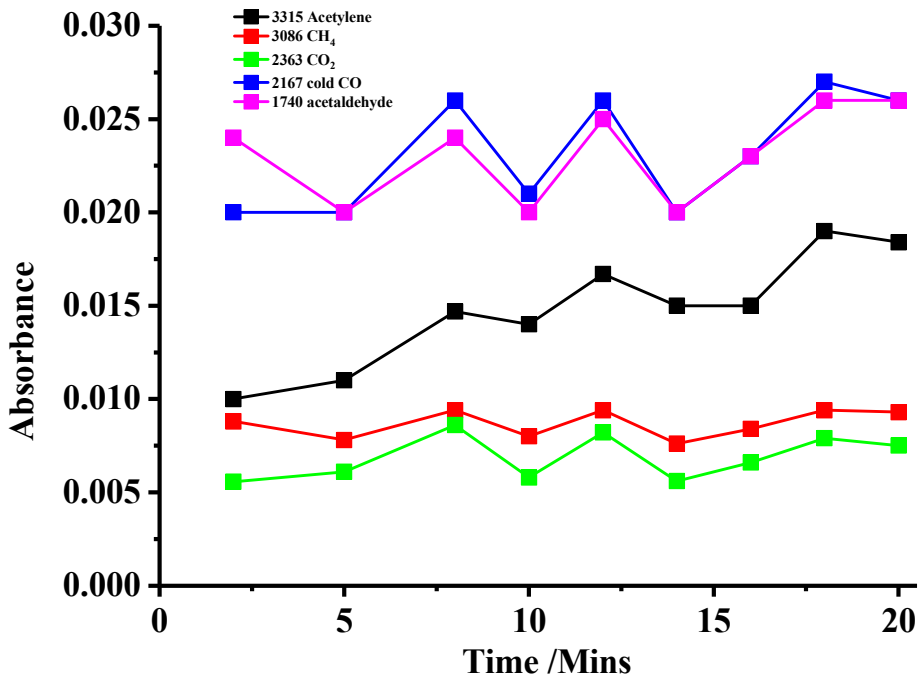

Figure 9. Plots of the intensities of the various features in Figure 8(a) as a function of time.

- It is clear from Figures 3 and 9 that CO, CH_4, HCN and acetone track each other exactly suggesting some commonality.

- Replacing N_2 by Ar not only removes HCN but results in the formation of acetylene.

The production of cold CO suggests the presence of a "loose" or "late" transition state and hence the possible presence of a roaming mechanism. The roaming mechanism was first proposed by van Zee et al. [75] in a seminal paper on the photolysis of formaldehyde to CO and H_2: in essence the standard, tight transition state route produced rotationally hot CO whilst the loose transition state resulted in rotationally cold CO. During the photolysis of acetaldehyde, the formation of a loose transition state allows a roaming mechanism that results in CH_4 and cold

CO[76-78], and work by the Klippenstein group[79,80] shows the same is true for thermal decomposition of CH_3CHO at T > 1000K.

It is not unreasonable to postulate acetaldehyde as an intermediate, however it is difficult to identify from IR spectra in the presence of acetone as it usually appears as a shoulder on the lower frequency of the acetone 1740 cm^{-1} C=O stretch. Further, in our case, it may be present at low steady state concentrations below the detection limit of the equipment. If acetaldehyde is the key intermediate then the following mechanism would explain the observed data.

As per the model proposed by Kim and co-workers[73], there are two reaction zones, the Macor/plasma interface and the bulk plasma, the chemistry in the latter wholly uninfluenced by the Macor.

In the bulk of the plasma, the formation of both acetaldehyde and acetone takes place via electron impact:

$$CH_3CHOHCH_3 + e^- \rightarrow CH_3CHO + CH_4 + e^- \quad (4)$$

$$CH_3CHOHCH_3 + e^- \rightarrow C_3H_7O^+ + H^+ + 3e^- \quad (5)$$

$$C_3H_7O^+ \rightarrow CH_3COCH_3 + H^+ \quad (6)$$

Other decomposition mechanisms are also possible such as reaction with excited metastable N_2 (e.g. $A^3\Sigma_u^+$) and atomic nitrogen such as in the following reaction:

$$CH_3CHOHCH_3 + N \rightarrow C_3H_7 + HNO \qquad (7)$$

Acetone does not react further: in contrast, acetaldehyde may react further, either by electron impact or photoexcitation (nitrogen-fed non-thermal plasmas show significant emission[81] around the λ_{max} for the dissociation of acetaldehyde of 308 nm[76])

$$CH_3CHO + e^- \rightarrow [CH_3\text{----}CHO]^{\ddagger} + e^- \text{ (Loose TS)} \qquad (8)$$

$$CH_3CHO + h\nu \rightarrow [CH_3\text{----}CHO]^{\ddagger} \text{ (Loose TS)} \qquad (9)$$

$$[CH_3\text{----}CHO]^{\ddagger} \rightarrow CH_4 + CO\text{(cold)} \text{ (Roaming)} \qquad (10)$$

$$[CH_3\text{--}CHO]^{\ddagger} \rightarrow CH_3 + CHO \text{ (Tight TS)} \qquad (11)$$

In the absence of the liquid film, i.e. with the Macor surface accessible, acetaldehyde is dehydrated to acetylene, catalysed by aluminium/magnesium oxide sites[82] on the Macor:

$$CH_3CHO \rightarrow HC{\equiv}CH + H_2O \qquad (12)$$

4. Conclusions

Macor does not catalyse any reaction of isopropyl alcohol in dinitrogen at temperatures up to 600°C. In contrast, it has a very significant effect upon the analogous plasma-driven process. In

N_2 + IPA –fed non-thermal plasma, two reaction zones are established: one at the Macor/plasma interface where the Macor catalyses the formation of a brown oil containing a polymethylacetylene-like polymer also (probably) bearing nitrogen containing functionality, and isophorone. This oil eventually blocks the Macor surface preventing further reactions of this nature. The second zone is in the bulk of the plasma, remote from the Macor. In this zone, CO at a rotational temperature << 200K and CH_4, HCN and acetone are also produced. Electron impact of the IPA results in acetone and acetaldehyde production: the former does not react further. In contrast, the acetaldehyde is excited to form a loose transition state via electron impact or photo-excitation from the plasma emission: this results in the dissociation of the acetaldehyde to CH_4 and cold CO via a roaming reaction. Replacing the dinitrogen by argon completely inhibits the formation of the oil, leaving the Macor surface clear, and this now catalyses the formation of acetylene.

Associated Content

SI Supporting Information

(a) A photograph and (b) schematic of the *in-situ* FTIR non thermal plasma cell (Figure S1), Comparison the spectra of gas phase IPA and an authentic sample of liquid IPA. The former was obtained using the plasma transmission cell, and the latter as a thin layer pressed between the CaF_2 windows of a Thermo Scientific Presslok demountable cell holder (Figure S2), The spectrum collected at 27W in Figure 1(a) and that of 13.4% CH_4+ 10.6% CO_2 + 76.0% N_2 in the plasma transmission cell (Figure S3), A spectrum of (i) gas phase acetone obtained in the plasma transmission cell and (ii) the spectrum in Figure 2(b): (a) full spectral range and (b) 900 – 2000

cm^{-1}. The acetone spectrum was reduced by a factor of 3.9 (Figure S4), (i) The CO spectral region of Figure S3 and (ii) that of a spectrum collected of 100% CO in a 1 cm pathlength transmission cell at 298K. The spectrum in (ii) has been scaled down by a factor of 15.7 (Figure S5), In-situ FTIR absorbance spectra (100 co-added scans and averaged scans at 4 cm^{-1} resolution, ca. 100 seconds per scan set) collected during the plasma treatment of IPA at 27W as a function of plasma operation time. The N_2 gas flow rate was 200 cm^3 min^{-1}, bubbled through a Dreschel bottle of pure IPA at room temperature (Figure S6), Plots of the intensities of the 2164 cm^{-1} CO band and the 1740 cm^{-1} acetone band, and the partial pressure of CO, measured after 1 minute plasma operation as a function of input power. The spectra were collected and manipulated as in the experiment shown in Figure 2(a) (Figure S7), Plot of the intensities of the key features in Figure 4 vs time (Figure S8), The spectra collected in Figure 4 up to 8 minutes (Figure S9), The spectrum collected after 8 minutes in Figure 4 subtracted from those taken up to 20 minutes (Figure S10), and IR spectrum of ca. 50 μL isophorone obtained as a thin layer pressed between the CaF_2 windows of a Thermo Scientific Presslok demountable cell holder (Figure S11).

Author Information

Corrresponding Author

Paul A. Christensen*[a]

E-mail: paul.christensen@ncl.ac.uk

Address: School of Engineering, Bedson Building, Newcastle University, Newcastle upon Tyne, NE1 7RU, UK.

Author Contributions

The manuscript was written through contributions of all authors. All authors have given approval to the final version of the manuscript.

Funding Sources

The authors declare no competing financial interest.

Acknowledgements

Abd Halim Bin Md Ali would like to thank the Government of Malaysia for a scholarship to study for a Ph. D, the staff of the Majlis Amanah Rakyat in Kuala Lumpur, Malaysia and London, United Kingdom for their invaluable assistance. Z. T. A. W. Mashhadani would like to thank the Government of Iraq for a Scholarship, the staff of the Higher Committee for Education Development in Iraq for their invaluable assistance and the Iraq Ministry of Oil Petroleum Research and Development Center PRDC for the opportunity to study for a Ph. D. The authors also wish to thank Mr. Neville Dickman for his assistance and support for this work and Prof. Bernard Golding for helpful discussions.

References

1. Gicquel, A.; Cavadias, S.; Amouroux, J. Heterogeneous Catalysis in Low-Pressure Plasmas. *J. of Phys. D: Appl. Phys.* **1986**, 19, 2013-2042.

2. Bahri, M.; Haghighat, F. Plasma-Based Indoor Air Cleaning Technologies: The State of the Art-Review. *CLEAN–Soil, Air, Water* **2014**, 42, 1667-1680.

3. Manley, T. C. The Electric Characteristics of the Ozonator Discharge. *ECST* **1943**, 84, 83-96.

4. Nozaki, T.; Muto, N.; Kado, S.; Okazaki, K. Dissociation of Vibrationally Excited Methane on Ni Catalyst: Part 1. Application to Methane Steam Reforming. *Cat. Today* **2004**, 89, 57-65.

5. Langleron, M.; Cavadias, S.; Amouroux, J. Study by Mass Spectrometry and Gas Chromatography of Toluene Oxidation in a Low-Pressure Plasma Reactor. *Rapid Commun. Mass Sp.* **1995**, 9, 18-22.

6. Jeong, J. Y.; Park, J.; Henins, I.; Babayan, S. E.; Tu, V. J.; Selwyn, G. S.; Hicks, R. F. Reaction Chemistry in the Afterglow of an Oxygen− Helium, Atmospheric-Pressure Plasma. *J Phys Chem A* **2000**, 104, 8027-8032.

7. Kasinathan, P.; Park, S.; Choi, W. C.; Hwang, Y. K.; Chang, J. S.; Park, Y. K. Plasma-Enhanced Methane Direct Conversion Over Particle-Size Adjusted MOx/Al_2O_3 (M= Ti and Mg) Catalysts. *Plasma Chem Plasma P.* **2014**, 34, 1317-1330.

8. Thejaswini, H. C.; Peglow, S.; Sushkov, V.; Hippler, R. Infrared Spectroscopy of CH_4/N_2 and C_2H_m/N_2 (m= 2, 4, 6) Gas Mixtures in a Dielectric Barrier Discharge. *Plasma Chem Plasma P.* **2014**, 34, 1157-1170.

9. Whitehead, J. C. Plasma–Catalysis: The Known Knowns, The Known Unknowns and The Unknown Unknowns. *J Phys D Appl Phys.* **2016**, 49, 243001 (24pp).

10. Chen, H. L.; Lee, H. M.; Chen, S. H.; Chang, M. B. Review of Packed-Bed Plasma Reactor for Ozone Generation and Air Pollution Control. *Ind Eng Chem Res.* **2008**, 47, 2122-2130.

11. Fridman, A. *Plasma Chemistry*; Cambridge University Press: New York, **2008**, p263.

12. Aerts, R.; Somers, W.; Bogaerts, A. Carbon Dioxide Splitting in a Dielectric Barrier Discharge Plasma: a Combined Experimental and Computational Study. *ChemSusChem.* **2015**, 8, 702 – 716.

13. Martuzevicius, D.; Denafas, G.; Stasiulaitienė, I.; Abromaitis, V.; Ochmanaitė, V; Krugly, E.; Prasauskas, T. Report on Eco-Efficiency of Plasma-Based Technologies for Environmental Protection, Kaunas **2011,** http://www.plastep.eu/fileadmin/dateien/Outputs/OP3-2.1_Eco-efficiency_report.pdf.

14. Hammer, T. Atmospheric Pressure Plasma Application for Pollution Control in Industrial Processes. *Contrib Plasm Phys.* **2014**, 54, 187 – 201.

15. Kogelschatz, U. Dielectric-Barrier Discharges: Their History, Discharge Physics, and Industrial Applications. *Plasma Chem Plasma P.* **2003**, 23, 1 – 46

16. Malik, M. A.; Hughes, D.; Heller, R.; Schoenbach, K. H. Surface Plasmas Versus Volume Plasma: Energy Deposition and Ozone Generation in Air and Oxygen. *Plasma Chem Plasma P.* **2015**, 35, 697 – 704.

17. Zhang, K.; Mukhriza, T.; Liu, X.; Greco, P. P.; Chiremba, E. A study on CO_2 and CH_4 Conversion to Synthesis Gas and Higher Hydrocarbons by the Combination of Catalysts and Dielectric-Barrier Discharges. *Appl Catal A Gen* **.2015**, 502, 138-149.

18. Nguyen, V. N.; Blum, L. Syngas and Synfuels From H_2O and CO_2: Current Status. *Chem Ing Tech.* **2015**, 87, 354 – 375.

19. Xiao, G.; Xu, W.; Wu, R.; Ni, M.; Du, C.; Gao, X.; Luo, Z.; Cen, K. Non-Thermal Plasmas For Vocs Abatement. . *Plasma Chem Plasma P.* **2014**, 34, 1033 – 1065

20. Scholtz, V.; Pazlarová, J.; Soušková, H.; Khuna, J.; Julá, J. Nonthermal Plasma—A Tool for Decontamination and Disinfection. *Biotechnol Adv.* **2015**, 33, 1108-1119.

21. Lili, B. A. N.; Ping, L. I. U.; Cunhua, M. A.; Bin, D. A. I. Deep Desulfurization of Diesel Fuels With Plasma/Air as Oxidizing Medium, Diperiodatocuprate (III) as Catalyzer and Ionic Liquid as Extraction Solvent. *Plasma Sci Technol.* **2013**, *15*(12), 1226-1231.

22. Bai1, M.; Leng, B.; Mao, S.; Li, C. Flue Gas Desulfurization by Dielectric Barrier Discharge. *Plasma Chem Plasma P.* **2016**, 36, 511 – 521.

23. Ashford, B.; Tu, X. Non-Thermal Plasma Technology for the Conversion of CO_2. *Curr Opin Environ Sustain.* **2017**, 3, 45 – 49.

24. Scarduelli, G.; Guella, G.; Ascenzi, D.; Tosi, P. Synthesis of liquid organic compounds from CH_4 and CO_2 in a dielectric barrier discharge operating at atmospheric pressure. *Plasma Process Polym.* **2011**, 8, 25 – 31.

25. Zeng, Y.; Zhu, X.; Mei, D.; Ashford, B.; Tu, X. Plasma-Catalytic Dry Reforming of Methane Over γ-Al_2 O_3 Supported Metal Catalysts. *Catal Today* **2015**, 256, 80 – 87.

26. De Bie, C.; van Dijk, J.; Bogaerts, A. The Dominant Pathways for the Conversion of Methane into Oxygenates and Syngas in an Atmospheric Pressure Dielectric Barrier Discharge. *J Phys Chem C* **2015**, 119, 22331 – 22350.

27. http://www.nap.edu/catalog/11960/plasma-science-advancing-knowledge-in-the-national-interest p29-32.

28. Neyts, E. C. Plasma-Surface Interactions in Plasma Catalysis. *Plasma Chem Plasma P.* **2016**, 36, pp.185 - 212.

29. Havran, V.; Dudukovic, M. P.; Lo, C. L. Conversion of Methane and Carbon Dioxide to Higher Value Products. *Ind Eng Chem Res.* **2011**, 50, 7089 – 7100.

30. Abd Allah, Z.; Whitehead, J. C.; Martin, P. Remediation of Dichloromethane (CH_2Cl_2) Using Non-Thermal, Atmospheric Pressure Plasma Generated in a Packed-Bed Reactor. *Environ Sci Technol.* **2013**, 48, 558-565.

31. Kozák, T.; Bogaerts, A. Splitting of CO_2 by Vibrational Excitation in Non-Equilibrium Plasmas: a Reaction Kinetics Model. *Plasma Sources Sci T.* **2014**, 23, 045004 (17pp).

32. Sakiyama, Y.; Graves, D. B.; Chang, H. W.; Shimizu, T.; Morfill, G. E. Plasma Chemistry Model of Surface Microdischarge in Humid Air and Dynamics of Reactive Neutral Species. *J Phys D Appl Phys.* **2012**, 45, 425201 (19pp).

33. Al-Abduly, A.; Christensen, P. A. An In Situ and Downstream Study of Non-Thermal Plasma Chemistry in an Air Fed Dielectric Barrier Discharge (DBD*). Plasma Sources Sci T.* **2015**, 24, 065006 (16pp).

34. Christensen, P. A.; Attidekou, P. S.; Egdell, R. G.; Maneelok, S.; Manning, D. A. C. An In Situ FTIR Spectroscopic And Thermogravimetric Analysis Study of the Dehydration and Dihydroxylation of SnO_2: the Contribution of the (100),(110) and (111) Facets. *Phys Chem Chem Phys.* **2016**, 18, 22990-22998.

35. https://psec.uchicago.edu/ceramics/MACOR%20Data%20Sheet.pdf.

36. Subrahmanyam, C.; Renken, A.; Kiwi-Minsker, L. Novel Catalytic Dielectric Barrier Discharge Reactor for Gas-Phase Abatement of Isopropanol. *Plasma Chem Plasma P.* **2007**, 27, 13-22.

37. Jarrige J.; Vervisch, P. Plasma-Enhanced Catalysis of Propane and Isopropyl Alcohol at Ambient Temperature on a MnO_2-Based Catalyst. *Appl Catal B* **2009**, 90, 74 - 82.

38. Leclerq, J.; Giraud, F.; Bianchi, D.; Fiaty, F.; Gaillard, F. Plasma-assisted Catalysis for the Abatement of Isopropyl Alcohol over Metal Oxides. *Appl Catal B* **2014**, 146, 131 – 137.

39. Miyata, H.; Wakamiya, M.; Kubokawa, Y. Infrared Studies of Interaction Of Oxygen With 2-Propanol and Acetone Adsorbed on MgO and NiO. *J Catal.* **1974**, 34, 117-123.

40. Koga, O.; Onishi, T.; Tamaru, K. Adsorption and Decomposition of Isopropyl Alcohol Over Zinc Oxide. Infrared and Kinetic Study. *J. Chem. Soc. Faraday Trans. 1* **1980**, 76, 19 – 29.

41. Rossi, P. F.; Busca, G.; Lorenzelli, V.; Saur, O.; Lavalley, J. C. Microcalorimetric and FT-IR Spectroscopic Study of the Adsorption of Isopropyl Alcohol and Hexafluoroisopropyl Alcohol on Titanium Dioxide. *Langmuir* **1987**, 3, 52 - 58.

42. Hussein, G. A. M.; Sheppard, N.; Zaki, M. I.; Fahim, R. B. Infrared Spectroscopic Studies of the Reactions of Alcohols Over Group IVB Metal Oxide Catalysts. Part 1.—Propan-2-ol Over TiO_2, ZrO_2 and HfO_2. *J. Chem. Soc. Faraday Trans. 1* **1989**, 85, 1723 – 1741.

43. Resini, C.; Montanari, T.; Busca, G.; Jehng, J-M.; Wachs, I. E. Comparison of Alcohol and Alkane Oxidative Dehydrogenation Reactions Over Supported Vanadium Oxide Catalysts:

In Situ Infrared, Raman and UV–Vis Spectroscopic Studies of Surface Alkoxide Intermediates and of Their Surface Chemistry. *Catal Today* **2005**, 99, 105–114.

44. Arsac, F.; Bianchi, D.; Chovelon, J. M.; Ferronato, C.; Herrmann, J. M. Experimental Microkinetic Approach of the Photocatalytic Oxidation of Isopropyl Alcohol on TiO2. Part 1. Surface Elementary Steps Involving Gaseous and Adsorbed C_3H x O Species. *J Phys Chem A* **2006**, 110, 4202 - 4212.

45. Xu, W.; Raftery, D.; Francisco, J. S. Effect of Irradiation Sources and Oxygen Concentration on the Photocatalytic Oxidation of 2-Propanol and Acetone Studied by In Situ FTIR. *J Phys Chem B* **2003**, 107, 4537 - 4544.

46. Fuentea, S. A.; Ferrettib, C. A.; Domancicha, N. F.; Díezb, V. K.; Apesteguíab, C. R.; Di Cosimob, J. I.; Ferulloc, R. M.; Castellani, N. J. Adsorption of 2-Propanol on MgO Surface: A Combined Experimental and Theoretical Study. *Appl Surf Sci.* **2015**, 327, 268–276.

47. Schmidt-Bleker, A.; Winter, J.; Iseni1, S.; Dünnbier, M.; Weltmann, K-D.; Reuter, S. Tracking Plasma Generated H_2O_2 From Gas Into Liquid Phase and Revealing Its Dominant Impact on Human Skin Cells. *J Phys D Appl Phys.* **2014**, 47, 145201 (12pp).

48. Rivallan, M.; Fourré, E.; Aiello, S.; Tatibouët, J-M.; Thibault-Starzyk, F. Insights into the Mechanisms of Isopropanol Conversion on γ-Al_2O_3 By Dielectric Barrier Discharge. *Plasma Process Polym.* **2012**, 9, 850-854.

49. Li, K.; Gabriel, O.; Meichsner, J. Fourier Transform Infrared Spectroscopy Study of Molecular Structure Formation in Thin Films during Hexamethyldisiloxane Decomposition in Low Pressure Rf Discharge. *Journal of Physics D: Applied Physics* **2004**, 37, 588 – 594.

50. Stere, C. E.; Adress, W.; Burch, R.; Chansai, S.; Goguet, A.; Graham, W. G.; Hardacre, C. Probing a Non-Thermal Plasma Activated Heterogeneously Catalyzed Reaction Using In Situ DRIFTS-MS. *ACS Catal.* **2015**, 5, 956 – 964.

51. Rodrigues, A.; Tatibouët, J-M.; Fourré, E. Operando DRIFT Spectroscopy Characterization of Intermediate Species on Catalysts Surface in VOC Removal from Air by Non-thermal Plasma Assisted Catalysis. *Plasma Chem Plasma P.* **2016**, 36, 901 – 905.

52. Jia, Z.; Rousseau, A. Sorbent Track: Quantitative Monitoring of Adsorbed VOCs Under In-Situ Plasma Exposure. *Nature Scientific reports* **2016**, 6, 31888, 1 – 11.

53. Rivallan, M.; Aiello, S.; Thibault-Starzyk, F. Operando DRIFT Spectroscopy Characterization of Intermediate Species on Catalysts Surface in VOC Removal from Air by Non-thermal Plasma Assisted Catalysis. *Rev. Sci. Instrum.* **2010**, 81, 103111(4 pp).

54. Barakat, C.; Gravejat, P.; Guaitella, O.; Thevenet, F.; Rousseau, A. Oxidation of Isopropanol and Acetone Adsorbed on TiO_2 Under Plasma Generated Ozone Flow: Gas Phase and Adsorbed Species Monitoring. *Appl Catal B* **2014**, 147, 302– 313.

55. P. A. Christensen, Abd Halim Bin Md Ali, Z. T. A. W. Mashhadani and P. A. Martin, A Direct Fourier Transform Infrared Spectroscopic Comparison of the Plasma- and Thermally-Driven Reaction of CO_2 at Macor. Plasma Chem Plasma Process, **2018**, 38: 293-310.

56. Choi, K. N.; Barker, E. F. Infrared Absorption Spectrum of Hydrogen Cyanide. *Phys. Rev.* **1932**, 42, 777-785.

57. Mehrotra, R. C.; Batwara, J. M. Preperation and Reactions of Alkoxides of Gadolinium and Erbium. *Inorg Chem.* **1970**, 9, 2595 – 2510.

58. Herzberg, G., *Infrared and Raman Spectra of Polyatomic Molecules*; D. Van Nostrand Company: New York, **1945**, pp 306 – 307.

59. Dellepiane, G.; Overend, J. Vibrational Spectra and Assignment of Acetone, ααα Acetone-d3 and Acetone-d6. *Spectrochim Acta.* **1966**, 22, 593 – 614.

60. Luyben, W. L. Design and Control of the Acetone Process via Dehydrogenation of 2-Propanol. *Ind Eng Chem Res.* **2011**, 50, 1206 – 1218.

61. Rioux, M.; Vannice, M. A. Hydrogenation/Dehydrogenation Reactions: Isopropanol Dehydrogenation over Copper Catalysts. *J Catal.* **2003**, 216, 362 – 376.

62. Said, A. E-A. A.; El-Wahib, M. M. M. A.; Goda, M. N. Selective Synthesis of Acetone from Isopropyl Alcohol Over Active and Stable CuO–NiO Nanocomposites at Relatively Low-Temperature. *Egy J Basic Appl Scis.* **2016**, 3, 357 – 365.

63. Halwy, S. A.; Mohamed, M. A.; El-Hafez, S. F. A. Dehydrogenation of Isopropyl Alcohol over Co Ni/Mg Oxide Catalysts. *J Mol Catal.* **1994**, 94, 191 – 201.

64. Tsang, C. W.; Harrison, A. G. Concerning the Structure and Fragmentation of $[C_3H_7O]$+ Ions Derived from Alcohols. *Journal of Mass Spectrometry* **1971**, 5, 877 – 884.

65. Bauerecker, S.; Taraschewski, M.; Weitkamp, C.; Cammenga, H. K. Liquid-Helium Temperature Long-Path Infrared Spectroscopy of Molecular Clusters and Supercooled Molecules. *Rev Sci Instrum.* **2001**, 72, 3946 - 3955.

66. Herzberg, G. *Molecular Spectra and Molecular Structure: I Spectra of Diatomic Molecules*, 2nd Edn., Van Nostrand, New York, **1950**, 126 – 127.

67. Cataldo, F. Synthesis of Ketonic Resins from Self-Polymerization of Acetone, 1. Action of Protic and Lewis Acids on Acetone. *Macromol Mater Eng.* **1996**, 236, 1-19.

68. Cataldo, F. Synthesis of Ketonic Resins from Self-Polymerization of Acetone, 2. Action Of Bases On Acetone And The Synthesis Of Halogenated And Diels-Alder Adducts. *Macromol Mater Eng.* **1996**, 236, 21-33.

69. Peluso, A.; Seel, M.; Ladik, J. The Infrared and Raman Spectrum of Trans-Polyacetylene: A Self-Consistent-Field Study. *Solid state commun.* **1985**, 53, 893 - 896.

70. Trinh, H. Q.; Mok, Y. S. Plasma-Catalytic Oxidation of Acetone in Annular Porous Monolithic Ceramic-Supported Catalysts. *Chem Eng J.* **2014**, 251, 199 - 206.

71. Manríquez, M. E.; Hernández-Cortez, J. G.; Wang, J. A.; Chen, L. F.; Zuñiga-Moreno, A.; Gómez, R. Synthesis of Transition Metal Doped Lamellar Double Hydroxides As Base Catalysts for Acetone Aldol Condensation. *Appl Clay Sci.* **2015**, 118, 188-194.

72. Giguère, P. A.; Harvey, K. B. On the Infrared Absorption of Water and Heavy Water in Condensed States. *Can J Chem*. **1956**, 34, 798-808.

73. Kim, H-H.; Teramoto, Y.; Negishi, N.; Ogata, A. A Multidisciplinary Approach to Understand the Interactions of Nonthermal Plasma and Catalyst: A Review. *Catal Today* **2015**, 256, 13 – 22.

74. Stein, S. E. "Infrared Spectra", NIST Chemistry WebBook, in NIST Standard Reference Database Number 69, Eds. P.J. Linstrom and W.G. Mallard, National Institute of Standards and Technology, Gaithersburg MD, 8860, http://webbook.nist.gov, (retrieved 24 October **2017**).

75. Van Zee, R. D.; Holtz, M. F.; Moore, C. B. Evidence for A Second Molecular Channel in the Fragmentation of Formaldehyde. *J Chem Phys.* **1993**, 99, 1664-1673.

76. Heazlewood, B. R.; Jordan, M. J. T.; Kable, S. H.; Selby, T. M.; Osborn, D. L.; Shepler, B. C.; Braams, B. J.; Bowman, J. M. Roaming is the Dominant Mechanism for Molecular Products in Acetaldehyde Photodissociation. *Proc Natl Acad Sci USA* **2008**, 105, 12719-12724.

77. Bowman, J. M. Skirting the Transition State, a New Paradigm in Reaction Rate Theory. *Proc Natl Acad Sci USA* **2006**, 103, 16079 – 16082.

78. Houston, P. L.; Cable, S. H. *Proc Natl Acad Sci USA* **2006**, 103, 16061 – 16062.

79. Sivaramakrishnan, R.; Michael, J. V.; Klippenstein, S. J. Direct Observation of Roaming Radicals in the Thermal Decomposition of Acetaldehyde. *J Phys Chem A* **2010**, 114, 755–764.

80. Harding, L. B.; Georgievskii, Y.; Klippenstein, S. J. Roaming Radical Kinetics in the Decomposition of Acetaldehyde. *J Phys Chem A* **2010**, 114, 765 – 777.

81. Xiao, D.; Cheng, C.; Shen, J.; Lan, Y.; Xie, H.; Shu, X.; Meng, Y.; Li, J.; Chu, P. K. Characteristics of Atmospheric-Pressure Non-Thermal N_2 And N_2/O_2 Gas Mixture Plasma Jet. *J. Appl. Phys.* **2014**, 115, 033303 (10pp).

82. Everett, C. Acetaldehyde Dehydration to Produce Ethyne, US 0102647 A1, May 27 **2004**.

TOC Graphic